

Influence of skin effect on the effective shielding effectiveness of composite materials

Valentin Préault, Romain Corcolle, Laurent Daniel, Lionel Pichon

▶ **To cite this version:**

Valentin Préault, Romain Corcolle, Laurent Daniel, Lionel Pichon. Influence of skin effect on the effective shielding effectiveness of composite materials. Journal of Applied Physics, 2014, 115 (15), pp.154904. 10.1063/1.4871197 . hal-01099336

HAL Id: hal-01099336

https://centralesupelec.hal.science/hal-01099336

Submitted on 22 Jul 2020

HAL is a multi-disciplinary open access archive for the deposit and dissemination of scientific research documents, whether they are published or not. The documents may come from teaching and research institutions in France or abroad, or from public or private research centers.

L'archive ouverte pluridisciplinaire **HAL**, est destinée au dépôt et à la diffusion de documents scientifiques de niveau recherche, publiés ou non, émanant des établissements d'enseignement et de recherche français ou étrangers, des laboratoires publics ou privés.

Journal of Applied Physics

Influence of skin effect on the effective shielding effectiveness of composite materials

Cite as: J. Appl. Phys. **115**, 154904 (2014); https://doi.org/10.1063/1.4871197
Submitted: 21 January 2014 . Accepted: 01 April 2014 . Published Online: 17 April 2014

Valentin Préault, Romain Corcolle, Laurent Daniel, and Lionel Pichon

View Online Export Citation CrossMark

ARTICLES YOU MAY BE INTERESTED IN

Experimental and computational study of shielding effectiveness of polycarbonate carbon nanocomposites
Journal of Applied Physics **120**, 145103 (2016); https://doi.org/10.1063/1.4964691

Electromagnetic interference shielding effectiveness of composite carbon nanotube macro-film at a high frequency range of 40 GHz to 60 GHz
AIP Advances **5**, 067130 (2015); https://doi.org/10.1063/1.4922599

A theory of electrical conductivity, dielectric constant, and electromagnetic interference shielding for lightweight graphene composite foams
Journal of Applied Physics **120**, 085102 (2016); https://doi.org/10.1063/1.4961401

Lock-in Amplifiers up to 600 MHz
Watch



AIP Publishing

© 2014 AIP Publishing LLC.

Influence of skin effect on the effective shielding effectiveness of composite materials

Valentin Préault,[1] Romain Corcolle,[1,a)] Laurent Daniel,[1,2] and Lionel Pichon[1]
[1]*Laboratoire de Génie Électrique de Paris, CNRS (UMR 8507)/SUPELEC/UPMC/Univ Paris-Sud, 11 rue Joliot-Curie, 91192 Gif sur Yvette, France*
[2]*School of Materials, University of Manchester, M13 9PL Manchester, United Kingdom*

(Received 21 January 2014; accepted 1 April 2014; published online 17 April 2014)

Composite materials are increasingly used to contribute to structure lightening in electromagnetic shielding applications. The interactions between electromagnetic waves and composite materials are highly dependent on their microstructure. This gives rise to challenging modelling issues. Considering details of the microstructure would involve an excessive number of unknowns with standard numerical tools for structural analysis. Homogenisation methods—such as Maxwell-Garnett model—are a possibility to overcome this problem. The equivalent homogeneous medium obtained with such methods can be introduced into numerical tools to model full shielding enclosures. A homogenisation model has been recently proposed to obtain the equivalent homogeneous properties of composite materials subjected to electromagnetic waves. It relies on the introduction of a length parameter into classical non dimensional semi-analytical homogenisation methods—also known as mean field approaches. The model is applicable at microwave frequencies as long as the induced currents in the fibres (or inclusions) of the composite materials remain weak. This paper proposes an extension of the approach to include skin effect in the homogenisation method. This is done by considering Joule losses within the fibres of the composite. This extension significantly broadens the frequency range covered by the model. The results show that the optimization of composite shielding properties relies on a subtle compromise between internal reflections and Joule losses. © *2014 AIP Publishing LLC*. [http://dx.doi.org/10.1063/1.4871197]

I. INTRODUCTION

Electromagnetic shielding enclosures contribute to electromagnetic compatibility. They are often made of metallic alloys. However, in the effort of reducing the weight of aircraft, the aerospace industry is considering the use of composite materials for shielding applications. Composites made of carbon fibres surrounded by epoxy resin are of particular interest.[1] Experimental studies have been performed on such composites but accurate modelling tools are still lacking for the optimal design of these new generation enclosures. Numerical methods such as the finite element method can be used.[2–8] These techniques are often performed on a periodic cell of the microstructure. This numerical homogenisation can be used to predict accurately the effective properties of the periodic cell. These effective properties can then be introduced in a structural analysis tool. If a large variety of electromagnetic loadings have to be considered, or if several microstructures have to be tested, these numerical methods can involve a significant computation cost, which can make them unsuitable, particularly in an engineering pre-design process.

An alternative approach is the use of semi-analytical homogenisation tools. Many homogenisation methods have been developed to model composite materials.[9–15] Although they sometimes make use of empirical parameters, they appear to be a very efficient and fast modelling tool to obtain a first estimate of the effective properties of heterogeneous materials. Maxwell-Garnett model (MGM) is frequently used to model composite materials submitted to electromagnetic waves, but it is limited to low frequencies. A Dynamic Homogenisation Model (DHM), providing the effective properties at higher frequencies, has been recently proposed.[16] An example of comparison between these two models and a standard Finite Element Model (FEM) is shown in Figure 1.

The figure is used here as an illustration of the motivations of this work, the simulation conditions are detailed in Sec. IV. If the FEM result is used as the reference, it can be seen in that example that MGM is only valid up to 2 GHz. The DHM increases the validity range up to 10 GHz, but then moves away from the FEM solution. These discrepancies at high frequency can be explained by the appearance of eddy currents in the conductive phase of the composite. The small inserts in Figure 1 show the electric field intensity in the cross-section of a fibre at three different frequencies (1, 10, and 60 GHz). MGM gets inaccurate as soon as a rotating electric field appears within the fibre. This can be understood by recalling that MGM is equivalent to Hashin and Shtrikman (HS) estimate, obtained from a variational principle.[17] HS estimate is known to be exact for a peculiar microstructure known as Hashin microstructure[10] for which the fields are uniform in one of the phases. It then seems natural that the HS model diverges from the exact solution as the inhomogeneity of fields increases. The validity range of the DHM is larger but the model also gets inaccurate when the skin-effect gets significant.

The skin effect in the inclusions appears to be a key parameter for the homogenisation methods at high frequency. The present paper proposes to account for this effect by a

a)Electronic mail: romain.corcolle@lgep.supelec.fr

 © 2014 AIP Publishing LLC

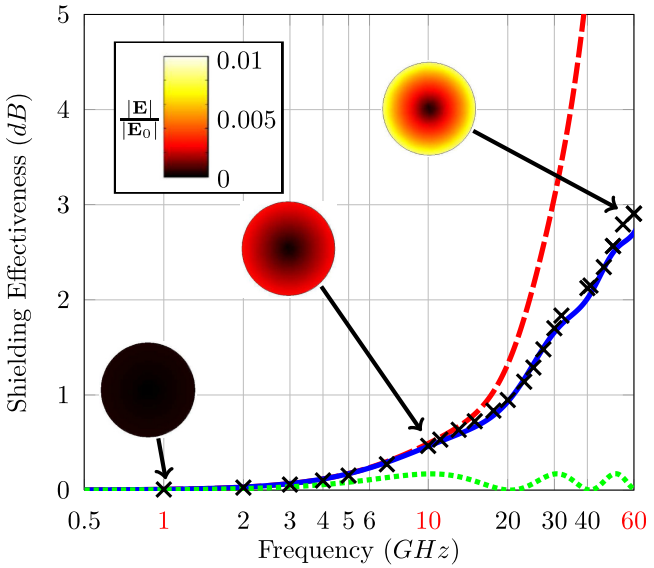


FIG. 1. Shielding Effectiveness of a composite material made of parallel fibres (index 2, diameter $\varnothing_2 = 50\,\mu$m, volume fraction $f_2 = 19.63\%$) embedded in a matrix (index 1). Computations performed on a periodic microstructure (Figure 4) with FEM (crosses), DHM (dashed line), EDHM (line), and MGM (dotted line). Constituent properties: $\sigma_1 = 1.10^{-15}\,\mathrm{S\cdot m^{-1}}$, $\sigma_2 = 40\,000\,\mathrm{S\cdot m^{-1}}$, $\epsilon_1 = \epsilon_2 = \epsilon_0$ and $\mu_1 = \mu_2 = \mu_0$.

modification of the DHM introducing the Joule losses. The results of this Extended Dynamic Homogenisation Model (EDHM) detailed hereafter shows an agreement with FEM up to high frequencies as shown in Figure 1. The EDHM is then applied in various configurations to demonstrate its validity range.

First, homogenisation methods based on inclusion problems are briefly recalled. A particular choice for the reference medium in the inclusion problems is then presented, based on an equivalence in Joule losses between this reference medium and the real material. The model is finally implemented and discussed by comparison to FEM results.

II. HOMOGENISATION MODEL

The purpose of homogenisation is to obtain the properties of an equivalent homogeneous medium (EHM) behaving—on average—similarly to the real heterogeneous material. The homogenisation method considered in this study is based on the resolution of inclusion problems.[18,19] There are as many inclusion problems as phases in the composite. Each phase is assumed to respond on average as an inclusion embedded in an homogeneous infinite medium (HIM). An appropriate choice of the HIM properties is key to the description of several types of microstructure. The shape of the representative inclusion is also a key parameter, related to the phase distribution in the composite material.[9,18]

A. Effective permittivity

For biphasic composites with isotropic constituents, if the HIM is chosen isotropic, the resolution of the two-inclusion problem provides the macroscopic complex permittivity $\tilde{\epsilon}^*_u$ of the EHM in direction $\mathbf{u}$[16]

$$\tilde{\epsilon}^*_u = \frac{\epsilon^*_1 \dfrac{f_1}{\epsilon^*_\infty + N_u(\epsilon^*_1 - \epsilon^*_\infty)} + \epsilon^*_2 \dfrac{f_2}{\epsilon^*_\infty + N_u(\epsilon^*_2 - \epsilon^*_\infty)}}{\dfrac{f_1}{\epsilon^*_\infty + N_u(\epsilon^*_1 - \epsilon^*_\infty)} + \dfrac{f_2}{\epsilon^*_\infty + N_u(\epsilon^*_2 - \epsilon^*_\infty)}}, \quad (1)$$

where ϵ^*_∞ is the complex permittivity of the HIM and N_u is the depolarisation factor along direction $\mathbf{u}$. For microstructures with infinitely long circular fibres, as studied in this paper, the depolarisation factors are $N_x = N_y = 1/2$ and $N_z = 0$. Equation (1) brings up the volume fraction f_i and the complex permittivity ϵ^*_i of phase i (Phase 1: matrix and Phase 2: fibres). The complex permittivities are written

$$\epsilon^*_i = \epsilon_i - \jmath\frac{\sigma_i}{\omega} \quad (2)$$

with ω the angular frequency, and ϵ_i and σ_i the electric permittivity and conductivity of the medium i.

B. Homogeneous infinite medium

Particular choices of the HIM allow retrieving the results of classical homogenisation models.[18,19] For instance, MGM can be obtained by choosing the matrix as the HIM ($\epsilon^*_\infty = \epsilon^*_1$). To extend the quasistatic approach to electromagnetic waves and form the DHM,[16] the infinite medium is chosen as

$$\epsilon^*_\infty = \epsilon^*_1 + \epsilon^*_2\left(\frac{\gamma}{\lambda}\right)^2, \quad (3)$$

where λ is the wavelength in the EHM and γ is the characteristic size of the microstructure. This characteristic size is a function of the considered microstructure. In the 2D case of a square array of conductive discs, γ is the diameter of the discs.[16] For more complex microstructures, γ can be determined by using 2-point probability functions.[20] This extension was proposed to address the absence of any length parameter in MGM. The ratio γ/λ is indeed a natural parameter to compare the characteristic length of the microstructure with the characteristic length of the electromagnetic wave. This size effect also depends on the fibre properties with higher effect in highly conductive materials. This is why ϵ^*_2 has been introduced in the definition of the infinite medium. Finally, ϵ^*_1 is introduced so that, at low frequencies (high λ), the model reduces to MGM (the second term in ϵ^*_∞ (3) vanishes).

As shown in Figure 1, the DHM overestimates the Shielding Effectiveness (SE). This is attributed to an overestimation of the effective conductivity of the composite material, leading to a higher attenuation of the electromagnetic wave. Such limitations have been overcome in previous studies by introducing a renormalised conductivity accounting for the Joule losses in the material.[21,22] In the present case, we choose to introduce the Joule losses in the definition of the HIM, using an *equivalent losses* conductivity (ELC) σ_∞

$$\epsilon^*_\infty = \epsilon^*_1 - \jmath\frac{\sigma_\infty}{\omega}. \quad (4)$$

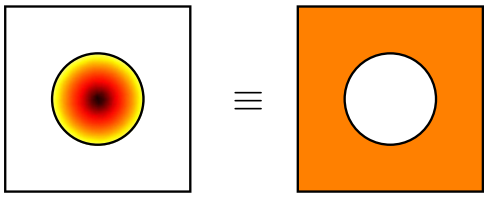


FIG. 2. Schematic view of the equivalence of energies.

As displayed on Figure 2, the ELC is computed so that the energy dissipated by a fibre is deported in the inclusion problem to the infinite medium with conductivity σ_∞.

The method is applied to 2D microstructures in the following. The extension to 3D microstructures requires more complex calculations for the Joule losses and is part of a work in progress.

III. JOULE LOSSES EQUIVALENCE

In order to define the proposed equivalence, the Joule losses in the real material are first computed analytically. The Joule losses in an infinite medium are then determined. Finally, the equivalence between these two energies defines the ELC.

A. Evaluation of Joule losses in the real material

1. Modelling configuration

The microstructure studied in this paper (Figure 4) is constituted of long parallel fibres (permittivity ϵ_2, conductivity σ_2, and permeability μ_2). To determine the energy lost in a fibre, the inner electromagnetic fields have to be computed. For the sake of simplicity, we use the semi-analytical expression computed for one fibre of the microstructure (Figure 3) surrounded by an homogeneous medium with properties (ϵ_s, μ_s). In the case of non-circular sections for the fibres, the diameter of an equivalent circular fibre, leading to the same Joule losses as the actual fibre, could be defined. Such equivalence can be defined analytically for elliptic sections but should rely on numerical computations for more complex shapes.

The fibre (radius R) is illuminated by an electromagnetic wave propagating along the **x** axis. However, only the induced currents rotating around **z** axis in the fibre are needed to compute Joule losses. Since the wavelength is greater than the diameter of the fibre, it is assumed that the fibre is embedded in a uniform magnetic field **H** in order to simplify the calculation

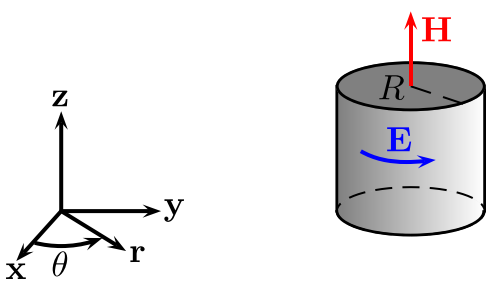


FIG. 3. Schematic view of a fibre.

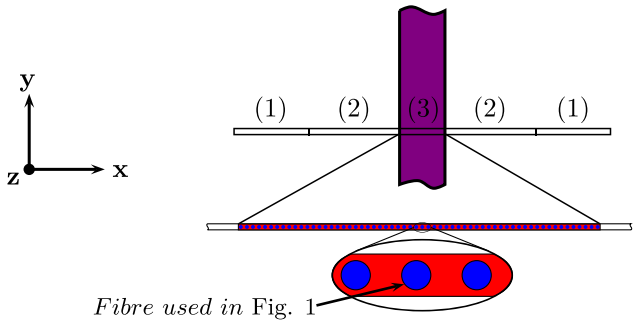


FIG. 4. Schematic view of SE computations configuration (including FEM domain: PML (1), Air (2) and studied sheet (3)) showing the fibre cross section used to measure the electric field plotted on Figure 1.

$$\mathbf{H}(r,\omega,t) = \begin{pmatrix} 0 \\ 0 \\ H_0 e^{\jmath\omega t} \end{pmatrix}_{(\mathbf{r},\theta,\mathbf{z})} \quad \text{for} \quad r > R. \tag{5}$$

2. Inner magnetic field

From Maxwell equations and the axisymmetry of the problem, the differential equation governing the magnetic field is

$$r^2 \frac{\partial^2 H_z(r,\omega,t)}{\partial r^2} + r \frac{\partial H_z(r,\omega,t)}{\partial r} + (rk_2)^2 H_z(r,\omega,t) = 0 \tag{6}$$

with $k_2 = \sqrt{\epsilon_2\mu_2\omega^2 - \jmath\mu_2\sigma_2\omega}$ the propagation constant in Phase 2. Bessel functions of the first and second kind of order zero are solutions of the differential Eq. (6). Since Bessel functions of the second kind are singular at the origin, they cannot be solution of the equation. The axial component of the internal magnetic field can finally be written

$$H_z(r,\omega,t) = H_0 \frac{\mathcal{J}_0(rk_2)}{\mathcal{J}_0(Rk_2)} e^{\jmath\omega t}, \tag{7}$$

where $\mathcal{J}_\alpha(x)$ is the Bessel function of the first kind of order α. Since the tangential component of the magnetic field is equal on both sides of the interface ($r = R$)

$$H_0 = \sqrt{\frac{\epsilon_s}{\mu_s}} E_0, \tag{8}$$

H_0 depends on the properties of the surrounding medium (ϵ_s, μ_s).

3. Inner electric field

The internal rotating electric field **E** induced by the magnetic field (7) is obtained from Maxwell-Ampère equation

$$E_\theta(r,\omega,t) = \frac{k_2}{\sigma_2 + \jmath\omega\epsilon_2} \sqrt{\frac{\epsilon_s}{\mu_s}} E_0 \frac{\mathcal{J}_1(rk_2)}{\mathcal{J}_0(Rk_2)} e^{\jmath\omega t}. \tag{9}$$

4. Induced currents

Using (9) and the linear constitutive law $\mathbf{J} = \sigma\mathbf{E}$, the equation of the azimuthal component of the induced currents (**J**) appearing inside the inclusion is easily deduced

$$J_\theta(r,\omega,t) = \frac{k_2}{1+\jmath\omega\frac{\epsilon_2}{\sigma_2}}\sqrt{\frac{\epsilon_s}{\mu_s}}E_0\frac{\mathcal{J}_1(rk_2)}{\mathcal{J}_0(Rk_2)}e^{\jmath\omega t}. \quad (10)$$

5. Joule losses

To take into account the influence of the whole microstructure, the surrounding medium (ϵ_s, μ_s) is chosen as the MGM effective medium $\epsilon_s = \frac{1+f_2}{f_1}\epsilon_1$ (see Appendix A) and $\mu_s = \mu_1$. The energy W_J^{Fibre} lost in a fibre by Joule effect over a period (see Appendix B) is given by

$$W_J^{Fibre} = 2\pi^2 h\epsilon_1\frac{1+f_2}{f_1}E_0^2\int_0^R r\left|\frac{\mathcal{J}_1(rk_2)}{\mathcal{J}_0(Rk_2)}\right|^2 dr, \quad (11)$$

where h is the height of the fibres. Note that the dependence of this energy to the fibre conductivity σ_2 is hidden in the expression of k_2. The surrounding medium being non-conductive, this expression of losses corresponds to the whole Joule losses in the unit cell (association of one fibre with volume fraction f_2 and surrounding medium).

B. Evaluation of Joule losses in the infinite medium

The local energy lost by an infinite isotropic homogeneous medium where there is an electric field $E = E_0 e^{\jmath\omega t}$ is equal to

$$w_J^\infty = \int_0^T J_\theta(r,\omega,t)E_\theta(r,\omega,t)dt = \frac{\pi}{\omega}\sigma_\infty E_0^2. \quad (12)$$

The energy lost by a volume of infinite medium equal to the volume ($\pi R^2 h/f_2$) of the unit cell considered in Sec. III A is

$$W_J^\infty = \frac{\pi R^2 h}{f_2}w_J^\infty = \frac{\pi^2 R^2 h}{f_2\,\omega}\sigma_\infty E_0^2. \quad (13)$$

C. Determination of the ELC

It is found that the best choice for the conductivity of the infinite homogeneous medium in the inclusion problem is obtained by deporting integrally the losses in the fibres to the infinite medium. This transfer is expressed by the equality

$$\frac{W_J^\infty}{f_1} = \frac{W_J^{Fibre}}{f_2}, \quad (14)$$

W_J^∞/f_1 and W_J^{Fibre}/f_2 are the losses in the HIM and in the fibres, respectively, scaled to their proportion in the inclusion problem. Introducing (11) and (13) in this equality leads to the following definition for the ELC

$$\frac{\sigma_\infty}{\omega} = \frac{2}{R^2}(1+f_2)\epsilon_1\int_0^R r\left|\frac{\mathcal{J}_1(rk_2)}{\mathcal{J}_0(Rk_2)}\right|^2 dr. \quad (15)$$

IV. MODELLING RESULTS

To evaluate the accuracy of the EDHM, the SE of a composite material sheet is compared to the SE of a homogeneous sheet with the EHM properties. The SE is classically defined by

$$SE = 20\log\frac{E_I}{E_T}, \quad (16)$$

where E_I and E_T are the norms of the incident and transmitted electric fields. The SE of the sheet made of the EHM is calculated analytically and the SE of the corresponding heterogeneous sheet is computed by FEM on a mesh of the complete microstructure as shown in Figure 4. We focus in the following on the case where the electric field is perpendicular to the fibres. An electric field parallel to the fibres does not allow a discriminating comparison since the Wiener estimate is generally sufficient to determine the SE in that particular case.[23]

A. Analytical solution for the shielding effectiveness

When the shielding sheet is illuminated by a perpendicular plane wave, the analytical solution of (16) can be expressed as (see Ref. 16)

$$SE = SE_A + SE_B - SE_R, \quad (17)$$

where SE_A is the attenuation of the wave caused by the absorption of the material

$$SE_A = 20\log_{10}|e^{\jmath kl}| \quad (18)$$

with $k = \sqrt{\epsilon\mu\omega^2 - \jmath\mu\sigma\omega}$. ϵ and σ are the permittivity and conductivity of the material in the direction of the incident electric field $\mathbf{E}_I$ and μ the magnetic permeability in the direction of the incident magnetic field $\mathbf{H}_I$. The second attenuation is caused by reflection

$$SE_R = 20\log_{10}|p|, \quad (19)$$

where $p = 4\frac{n}{\mu}/(\frac{n}{\mu}+1)^2$ is the transmission coefficient depending on $n = k/k_0$, the refractive index of the medium. The third contribution corresponds to multiple reflections inside the material

$$SE_B = 20\log_{10}|1 - q^2 \times e^{-2\jmath kl}|, \quad (20)$$

where $q = (\frac{n}{\mu}-1)/(\frac{n}{\mu}+1)$ is the reflection coefficient.

B. Finite element calculations

Due to computational resources limitations, numerical calculations have been processed on a small domain having a height of 0.1 mm (Figure 4) using COMSOL Multiphysics®. To simulate infinity, this domain is bounded by two perfectly matched layers (PMLs). Neumann boundary conditions are applied on top and bottom of the region modelled to simulate the periodicity of the infinite sheet. The sheet is 6 mm thick and filled with a single row of 60 cylindrical fibres (circular cross section), regularly spaced. These fibres have a diameter of 50 μm leading to a fibre volume fraction $f_2 = 19.63\%$. No contrast in permeability is considered ($\mu_1 = \mu_2$). The incident electromagnetic wave is a

perpendicular plane wave propagating along the **x** axis, electrically polarised along **y**. For a given frequency, the computation time with FEM is about 45 s on a standard workstation. The homogenisation model only takes some milliseconds on the same workstation.

As already shown in Figure 1, the DHM,[16] with HIM defined by (3), increases the frequency range of MGM but gets inaccurate when the skin effect becomes significant. The EDHM, with HIM defined by (4), still provides an accurate estimate at high frequencies when compared to FEM results. The case studied here gives a null SE at low frequencies because the matrix is not conductive. Results for MGM and DHM with a conductive matrix can be found in Ref. 20.

The EDHM can be used with various constituent properties. An example is shown in Figure 5. The microstructure is the same as in Figure 1, and the material properties are those used by De Rosa *et al.*[24] for the design of a composite made of short carbon fibres embedded in an epoxy resin.

All three models reproduce the oscillations of the SE as a function of the frequency. These oscillations are due to the multiple reflections of the wave on the material-air interface. These reflections depend on the thickness of the sheet and on the complex permittivity of the material. The SE tends to increase with frequency because the Joule losses increase with frequency. This effect is linked to the role of the effective conductivity of the composite, which is underestimated by the MGM, and overestimated by the DHM. The predictions of the EDHM are in good agreement with the FEM computations.

V. DISCUSSION

In order to assess the validity of the proposed EDHM, calculations have been performed under various configurations in terms of fibre diameter, fibre conductivity, fibre volume fraction, and matrix permittivity.

Figure 6 shows the difference between the homogenisation results (MGM, DHM, and EDHM) and the FEM results for the computations performed in this paper. Each marker represents the error with respect to the FEM computation calculated for a given set of parameters (frequency, fibre density, fibre diameter, fibre conductivity, and matrix permittivity). The results are plotted as a function of the ratio between the diameter of the fibres and the skin depth in a fibre ($\delta_2 = \sqrt{2/\mu_2\sigma_2\omega}$). The discrepancy between MGM and FEM results increases as soon as the skin depth of the fibre becomes equal to the diameter of the fibres $Ø_2$. As shown in Ref. 16, the DHM extends MGM frequency range until δ_2 becomes approximately equal to the radius of the fibres. The error then increases significantly. The error given by the EDHM increases slowly, the results staying relevant up to high ratios between the diameter and the skin depth of the fibres. It is clear from Figure 6 that the proposed approach significantly extends the frequency validity range of semi-analytical homogenisation method for the prediction of the SE of composite materials.

Figure 7 shows the results obtained with the EDHM and the FEM for different fibre diameters, the other properties being kept constant. The agreement is very good between the two methods although slight differences appear for the diameter of 100 μm. These differences can be attributed to the fact that for high fibre diameters, the problem computed with FEM is not really a Representative Volume Element. If the finite element calculation was done on a larger surface including more fibres, it is expected that the two results would be closer. Another cause could be an insufficient precision in the definition of the permittivity of the HIM. Indeed it can be shown that a better match could be obtained between EDHM and FEM with a slight change in the real

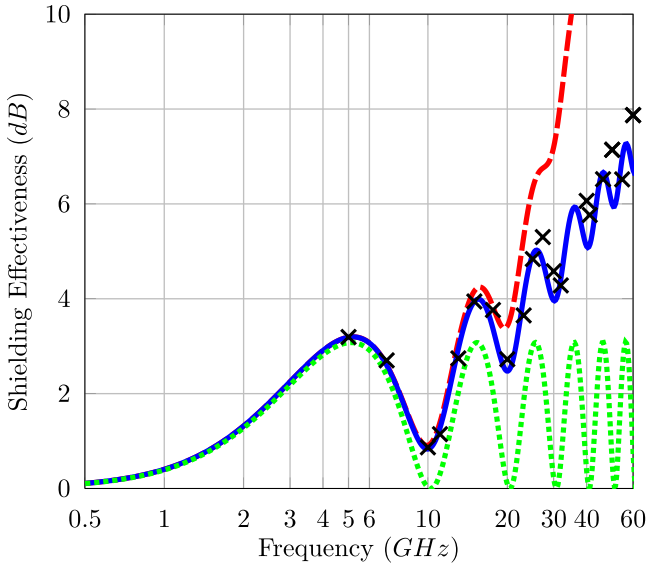


FIG. 5. Shielding Effectiveness of a composite material made of parallel fibres (index 2, diameter $Ø_2 = 50\,\mu$m, volume fraction $f_2 = 19.63\%$) embedded in a matrix (index 1). Computations performed on a periodic microstructure (Figure 4) with FEM (crosses), DHM (dashed line), EDHM (line), and MGM (dotted line). Constituent properties: $\sigma_1 = 1.10^{-15}$ S·m^{-1}, $\sigma_2 = 40\,000$ S·m^{-1}, $\epsilon_1 = 4\epsilon_0$, $\epsilon_2 = 2\epsilon_0$, and $\mu_1 = \mu_2 = \mu_0$.

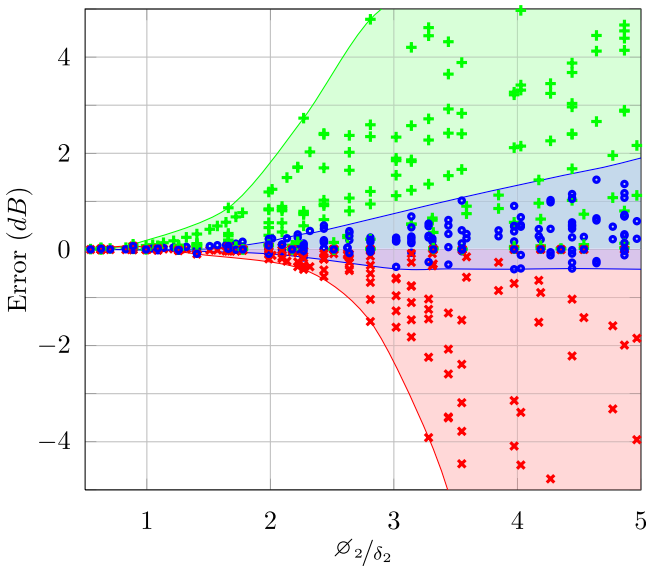


FIG. 6. Difference between the Shielding Effectiveness computed by MGM (+), the DHM (x), and EDHM (o) and the Shielding Effectiveness computed by FEM for the computations presented in this article. The coloured lines and the shaded areas show the envelope and the range of error obtained with each modelling approach.

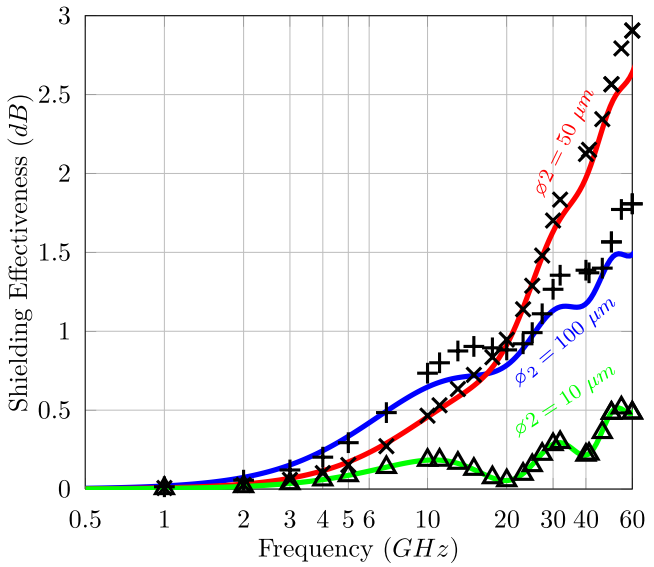


FIG. 7. Shielding Effectiveness of three composite materials made of parallel identical fibres (index 2, volume fraction $f_2 = 19.63\%$) with various diameters ($Ø_2$: 100 μm, 50 μm, and 10 μm) embedded in a matrix (index 1). Computations performed on periodic microstructures (see Figure 4) with FEM (markers) and EDHM (lines). Constituent properties: $\sigma_1 = 1.10^{-15}$ $S \cdot m^{-1}$, $\sigma_2 = 40\,000\,S \cdot m^{-1}$, $\epsilon_1 = \epsilon_2 = \epsilon_0$, and $\mu_1 = \mu_2 = \mu_0$.

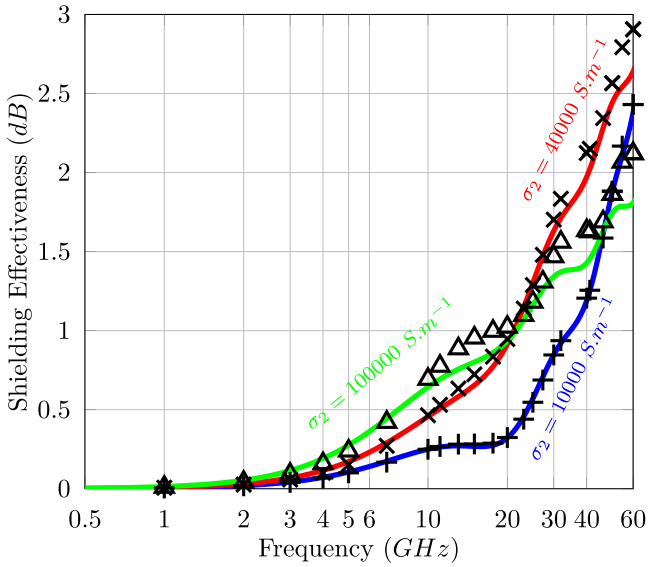


FIG. 8. Shielding Effectiveness of a composite material made of parallel fibres (index 2, diameter $Ø_2 = 50\,\mu$m, volume fraction $f_2 = 19.63\%$) embedded in a matrix (index 1). Computations performed on a periodic microstructure (Figure 4) with FEM (markers) and EDHM (lines) for various conductivities of fibres σ_2. Constituent properties: $\sigma_1 = 1.10^{-15}$ $S \cdot m^{-1}$, $\epsilon_1 = \epsilon_2 = \epsilon_0$, and $\mu_1 = \mu_2 = \mu_0$.

part of the HIM properties (4). This point highlights the crucial role played by the choice of the infinite medium in homogenisation approaches based on inclusion problems. Other definitions of the HIM properties can be investigated but the proposed choice (4) is the best obtained so far in terms of accuracy and versatility.

Another interesting observation is that the quality of the SE is not a monotonic function of the fibre diameters. If a high diameter is chosen, the skin effect appears at lower frequencies, inducing a better SE. But on the other hand at high frequency, the inner part of the fibres is free from currents since the skin effect tends to move the rotating currents towards the edge of the fibres. The area with no current is then larger with a large-fibre microstructure, creating relatively low Joule losses, and as a consequence decreasing the SE compared to small-diameter microstructures. The choice of an optimal diameter for the fibres of shielding composites is then a compromise between these two competitive processes.

Figure 8 shows the results obtained with the EDHM and the FEM for different fibre electric conductivities, the other properties being kept constant. The agreement is again very satisfying although differences appear for high fibre conductivity. These differences can here again be attributed to the choice of the properties for the HIM. The oscillations as a function of the frequency are very sensitive to the value of the HIM permittivity. A solution could be to describe the dependence of this permittivity to the fibre conductivity. This aspect will be investigated in future works.

Again it can be noted that the SE is not a monotonic function of the fibre conductivity. At low frequency, induced currents appear faster in high conductivity fibres. In such conditions, the higher fibre conductivity gives the higher conductivity for the effective medium, and as a consequence the best SE. But at high frequency, the skin effect gets more and more significant and high conductivity fibres create less Joule losses, which is then unfavourable for SE. This effect is included in the EDHM through the choice of the infinite medium (15) that is less conductive when Joule losses are lower. Again, the choice of the optimal properties for the fibres is a compromise between these two competitive processes.

Figure 9 shows the results obtained with the EDHM and the FEM for different fibre volume fractions, the other properties being kept constant. The agreement between FEM and EDHM is very satisfying. At high volume fractions, small

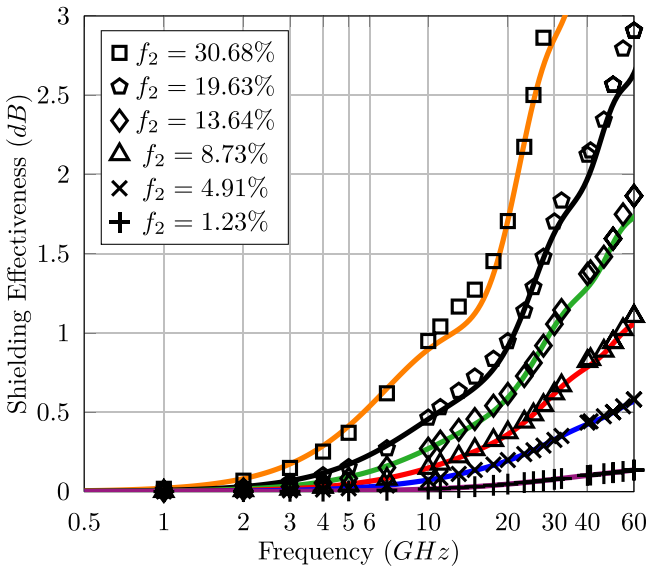


FIG. 9. Shielding Effectiveness of six composite materials made of parallel identical fibres (index 2, diameter $Ø_2 = 50\,\mu$m) embedded in a matrix (index 1). Computations performed on periodic microstructures (as Figure 4) with FEM (markers) and EDHM (lines) for various amount of fibre f_2. Constituent properties: $\sigma_1 = 1.10^{-15}$ $S \cdot m^{-1}$, $\sigma_2 = 40\,000\,S \cdot m^{-1}$, $\epsilon_1 = \epsilon_2 = \epsilon_0$, and $\mu_1 = \mu_2 = \mu_0$.

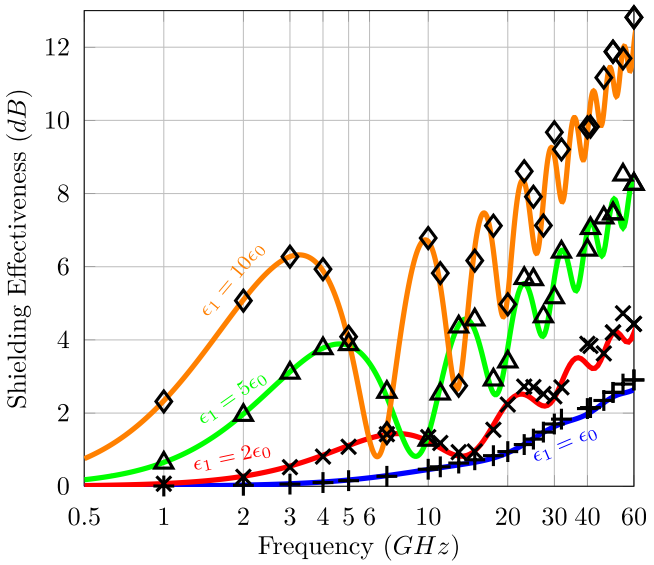


FIG. 10. Shielding Effectiveness of a composite material made of parallel fibres (index 2, diameter $\varnothing_2 = 50\,\mu$m, volume fraction $f_2 = 19.63\%$) embedded in a matrix (index 1). Computations performed on a periodic microstructure (Figure 4) with FEM (markers) and EDHM (lines) for three different permittivities of matrix ϵ_1. Constituent properties: $\sigma_1 = 1.10^{-15}$ S·m^{-1}, $\sigma_2 = 40\,000$ S·m^{-1}, $\epsilon_2 = \epsilon_0$, and $\mu_1 = \mu_2 = \mu_0$.

differences appear. They can be linked to the choice of Maxwell-Garnett approach for the choice of the infinite medium. This kind of approach is known to be valid only for small volume fractions.[18] At high volume fractions, a self-consistent approach would probably give a better agreement. The implementation of a self-consistent approach will be proposed in a further communication. As expected, Figure 9 shows that the higher the proportion of fibres, the better the SE.

Figure 10 shows the results obtained with the EDHM and the FEM for different matrix permittivities, the other properties being kept constant. The agreement between FEM and EDHM is very satisfying. The role of the matrix permittivity on the effective properties is rather complex. It affects both the effective permittivity and the effective conductivity. A high matrix permittivity increases the conductivity of the infinite medium (15), tending to increase the SE. On the other hand, the multiple reflections in the sheet heavily depend on the permittivity and on the frequency (20). A high matrix permittivity tends to increase the level of oscillations of SE as a function of frequency. This effect is well reproduced in Figure 10.

VI. CONCLUSION

In this paper, a semi-analytical homogenisation approach for the definition of the shielding effectiveness of composite materials is proposed. Contrarily to previous approaches, it is shown to be valid for electromagnetic waves at high frequencies—up to tens of GHz in the examples provided. The model is based on the resolution of basic inclusion problems. An appropriate choice of the infinite medium surrounding these inclusions is key to these approaches. A choice accounting for the Joule losses in the fibres is used for the proposed model. The results show very good agreement with finite element computations performed independently—and at much higher computational cost. An interesting outcome of the study is that contrarily to shielding sheets made of homogeneous materials where a conductivity as high as possible is sought in order to maximise the reflection effects, the choice of an optimal composite material for shielding effectiveness is a more subtle process. A compromise must be found between reflection effects and Joule losses within the fibres in order to maximise the overall shielding effectiveness. The proposed homogenisation method is a convenient tool to reach such an optimum, and can be readily used for pre-design process or for an implementation into standard numerical tools of full devices with complex geometries.

ACKNOWLEDGMENTS

The authors are grateful for support provided by the French government under the grant FUI-AAP10 SYRENA.

APPENDIX A: MAXWELL-GARNETT ESTIMATE

The Maxwell-Garnett estimate is intensively used in this paper. In 2 dimensions, Maxwell-Garnett model is usually written

$$\tilde{\epsilon}^*_{MG} = \epsilon^*_1 + 2f_2\epsilon^*_1 \frac{\epsilon^*_2 - \epsilon^*_1}{\epsilon^*_1(1+f_2) + f_1\epsilon^*_2}. \tag{A1}$$

In the case studied in this paper, the matrix (index 1) is non conductive, so that

$$\epsilon^*_1 = \epsilon_1, \tag{A2}$$

$$\epsilon^*_2 = \epsilon_2 - \jmath\frac{\sigma_2}{\omega}. \tag{A3}$$

By considering (A4) and (A3), (A1) can be written

$$\tilde{\epsilon}^*_{MG} = \epsilon_1 + 2f_2\epsilon_1 \frac{(\epsilon_2 - \epsilon_1) - \jmath\frac{\sigma_2}{\omega}}{(\epsilon_1(1+f_2) + f_1\epsilon_2) - f_1\jmath\frac{\sigma_2}{\omega}}. \tag{A4}$$

In the particular case of this article, the conductivity of fibres (index 2) is very high. This leads to $\sigma_2/\omega \gg \epsilon_1$ and ϵ_2. In such conditions, the previous expression for the Maxwell-Garnett model can be simplified. The real part is given by

$$\tilde{\epsilon}_{MG} \approx \epsilon_1 \frac{1+f_2}{f_1} \tag{A5}$$

and the imaginary part by

$$\frac{\tilde{\sigma}_{MG}}{\omega} \approx \omega 4 f_2 \frac{\epsilon_1^2}{f_1^2\sigma_2} \ll \tilde{\epsilon}_{MG}. \tag{A6}$$

The conductivity of the Maxwell-Garnett medium can then be neglected, and its permittivity can be written according to (A5).

APPENDIX B: JOULE LOSSES IN A FIBRE

The local energy lost by Joule effect w_J^{Fibre} in a fibre (ϵ_2 and μ_2) surrounded by an homogeneous medium (ϵ_s and μ_s) over a period ($T = 2\pi/\omega$) is computed by

$$w_J^{Fibre} = \int_0^T J_\theta(r,\omega,t)E_\theta(r,\omega,t)dt, \tag{B1}$$

$$w_J^{Fibre} = \frac{\pi}{\omega}\sigma_2\left|E_\theta(r,\omega,t)\right|^2, \tag{B2}$$

$$w_J^{Fibre} = \frac{\pi}{\omega}\sigma_2\left|\frac{k_2}{\sigma_2+j\omega\epsilon_2}\right|^2\left|\frac{\epsilon_s}{\mu_s}\right|\left|E_0^2\right|\left|\frac{\mathcal{J}_1(rk_2)}{\mathcal{J}_0(Rk_2)}\right|^2, \tag{B3}$$

$$w_J^{Fibre} = \frac{\pi}{\omega}\sigma_2\left|\frac{-\mu_2^2\omega^2}{-j\mu_2\sigma_2\omega}\right|\left|\frac{\epsilon_s}{\mu_s}\right|\left|E_0^2\right|\left|\frac{\mathcal{J}_1(rk_2)}{\mathcal{J}_0(Rk_2)}\right|^2. \tag{B4}$$

Equation (B4) can be simplified by considering the fibres highly conductive ($\sigma_2/\omega \gg \epsilon_2$), and by choosing the Maxwell-Garnett estimate for the surrounding medium ($\epsilon_s = \frac{1+f_2}{f_1}\epsilon_1$ and $\mu_s = \mu_1 = \mu_2$)

$$w_J^{Fibre} \approx \pi\epsilon_1\frac{1+f_2}{f_1}E_0^2\left|\frac{\mathcal{J}_1(rk_2)}{\mathcal{J}_0(Rk_2)}\right|^2. \tag{B5}$$

The total losses W_J^{Fibre} are computed by integrating the local energy over the radius since the integrated fields only depends on **r**

$$W_J^{Fibre} = h\int_0^R 2\pi r w_J^{Fibre}dr, \tag{B6}$$

$$W_J^{Fibre} \approx 2\pi^2 h\epsilon_1\frac{1+f_2}{f_1}E_0^2\int_0^R r\left|\frac{\mathcal{J}_1(rk_2)}{\mathcal{J}_0(Rk_2)}\right|^2 dr, \tag{B7}$$

where h is the height of the fibres.

[1]F. Qin and C. Brosseau, J. Appl. Phys. **111**, 061301 (2012).
[2]H. Waki, H. Igarashi, and T. Honma, IEEE Trans. Magn. **42**(4), 847 (2006).
[3]C. Cyr, P. Viarouge, S. Clénet, and J. Cros, IEEE Trans. Magn. **45**(3), 1178 (2009).
[4]O. Bottauscio, M. Chiampi, and A. Manzin, IEEE Trans. Magn. **45**(10), 3946 (2009).
[5]I. Niyonzima, R. V. Sabariego, P. Dular, and C. Geuzaine, IEEE Trans. Magn. **48**(2), 587 (2012).
[6]A. Bordianu, O. de la Barrière, O. Bottauscio, M. Chiampi, and A. Manzin, IEEE Trans. Magn. **48**(4), 1537 (2012).
[7]G. Wasselynck, D. Trichet, and J. Fouladgar, IEEE Trans. Magn. **49**(5), 1825 (2013).
[8]O. Ouchetto, H. Ouchetto, S. Zouhdi, and A. Sekkaki, IEEE Trans. Antennas Propag. **61**(8), 4214 (2013).
[9]A. Sihvola, *Electromagnetic Mixing Formulas and Applications* (IEE Electromagnetic Waves Series, 1999), p. 47.
[10]G. W. Milton, *The Theory of Composites* (Cambridge University Press, 2002).
[11]E. F. Kuester and C. L. Holloway, IEEE Trans. Microw. Theory Techn. **38**(11), 1752 (1990).
[12]C. Brosseau, J. Phys. D: Appl. Phys. **39**, 1277 (2006).
[13]M. Y. Koledintseva, J. Drewniak, R. Dubroff, K. Rozanov, and B. Archambeault, PIERB **15**, 197 (2009).
[14]S. El Bouazzaoui, M. E. Achour, and C. Brosseau, J. Appl. Phys. **110**, 074105 (2011).
[15]M. S. Sarto, A. G. D'Aloia, A. Tamburrano, and G. De Bellis, IEEE Trans. Electromagn. Compat. **54**(1), 17 (2012).
[16]V. Préault, R. Corcolle, L. Daniel, and L. Pichon, IEEE Trans. Electromagn. Compat. **55**(6), 1178 (2013).
[17]Z. Hashin and S. Shtrikman, J. Appl. Phys. **33**, 3125 (1962).
[18]M. Bornert, T. Bretheau, and P. Gilormini, *Homogénéisation en mécanique des matériaux* (Hermes Science, 2001).
[19]L. Daniel and R. Corcolle, IEEE Trans. Magn. **43**(7), 3153 (2007).
[20]V. Préault, R. Corcolle, L. Daniel, and L. Pichon, IEEE Trans. Magn. **49**(5), 1941 (2013).
[21]A. N. Lagarkov and A. K. Sarychev, Phys. Rev. B **53**(9), 6318 (1996).
[22]M. Y. Koledintseva, R. E. DuBroff, and R. W. Schwartz, PIER **63**, 223 (2006).
[23]J. A. Stratton, *Electromagnetic Theory* (McGraw-Hill, 1941).
[24]I. M. De Rosa, R. Mancinelli, F. Sarasini, M. S. Sarto, and A. Tamburrano, IEEE Trans. Electromagn. Compat. **51**(3), 700 (2009).